A Comparative Study of the Mass and Heat Transfer Dynamics of Evaporating Ethanol/Water, Methanol/Water, and 1-Propanol/Water Aerosol Droplets

Rebecca J. Hopkins and Jonathan P. Reid

School of Chemistry, University of Bristol, Cantock's Close, Bristol BS8 1TS, UK

Received: November 11, 2005; In Final Form: December 22, 2005

The mass and heat transfer dynamics of evaporating multicomponent alcohol/water droplets have been probed experimentally by examining changes in the near surface droplet composition and average droplet temperature using cavity-enhanced Raman scattering (CERS) and laser-induced fluorescence (LIF). The CERS technique provides a sensitive measure of the concentration of the volatile alcohol component in the outer shell of the droplet, due to the exponential relationship between CERS intensity and species concentration. Such volatile droplets, which are probed on a millisecond time scale, evaporate nonisothermally, resulting in both temperature and concentration gradients, as confirmed by comparisons between experimental measurements and quasi-steady state model calculations. An excellent agreement between the experimental evaporation trends and quasi-steady state model predictions is observed. An unexpectedly slow evaporation rate is observed for the evaporation of 1-propanol from a multicomponent droplet when compared to the model; possible explanations for this observation are discussed. In addition, the propagation depth of the CERS signal, and, therefore, the region of the droplet from which compositional measurements are made, can be estimated. Such measurements, when considered in conjunction with quasi-steady state theory, can allow droplet temperature gradients to be measured and vapor pressures and activity coefficients of components within the droplet to be determined.

1. Introduction

Aerosol particles have been the subject of much interest in recent years due to their importance in a diverse range of scientific disciplines including atmospheric chemistry and physics, combustion science, and their impact on human health.[1−4] The mass and heat transfer rates associated with the evaporation or growth of an aerosol particle are governed by the interaction between the gas and condensed phases. Thus, to gain a full understanding of mass and heat transfer processes, detailed experimental measurements are required that provide information on the evolving composition, size, temperature, and phase of an aerosol particle and their dependence on the composition and temperature of the gas phase. The majority of experimental studies to date performed on single aerosol particles have probed mass transfer by monitoring changes in particle mass, phase, and size, using both elastic light scattering and fluorescence methods. The evaporation of single component and multicomponent liquid aerosol droplets have been investigated with both volatile and nonvolatile constituents.[5−8] The evaporation of multiphase droplets consisting of two immiscible liquids has received some attention and the influence of surfactants on evaporation rates has been investigated.[9−11] Raman spectroscopy has mostly failed to provide a quantitative measure of the evolving particle composition, and only a few examples of compositional measurements have been possible.[12−16]

The evaporation and growth of a multicomponent droplet depends on kinetic and thermodynamic parameters, including the gas and liquid-phase diffusion coefficients, and the activity coefficients and vapor pressures of the constituents. The advent of particle trapping techniques such as electrodynamic, acoustic, and optical levitation methods has enabled the evolving size of a levitated droplet of low volatility to be monitored on time scales of minutes to hours.[17] Experiments have been performed on single droplets suspended in an electrodynamic balance to extract vapor−liquid equilibrium data[18,19] and to investigate the hygroscopic behavior of inorganic aerosol and the effect of organic components.[20,21] The evaporation of pure and multicomponent droplets of low vapor pressure proceeds isothermally, and the droplet surface temperature remains close to the ambient temperature. Evaporation can be described by considering mass transfer alone, and this is described by steady state theory. The activity coefficients of water in salt solutions have been determined by measuring the mass change of a suspended salt particle when equilibrium is attained with the surrounding vapor phase of a known activity.[22,23] This method has been applied not only to involatile solutes dissolved in volatile solvents, but also in measurements of the activity of water in droplets containing an evaporating soluble organic component.[24]

Rapid processes, such as the evaporation of volatile species occurring on time scales of <20 ms, have been investigated in droplet trains.[7,25−28] During evaporation the temperature of the interfacial region decreases below that of the surrounding gas phase. This regime is characterized by unsteady theory, and it is necessary to solve the coupled mass and energy conservation equations simultaneously.[26] This full treatment can be simplified by applying the quasi-steady-state approximation, which will be described in detail later.[29−31] Under unsteady conditions, Ray and co-workers have used elastic and Raman scattering spectra to determine the change in droplet size and refractive index as a function of time.[25,26] Using an unsteady-state model, they determined activity coefficients for ethanol and methanol evaporating from droplets in a train over short time periods. They observed a change in the rate of evaporation with time, a characteristic of an unsteady-state evaporation process. The refractive index at the surface of the droplet was measured,

10.1021/jp056523g CCC: $33.50 © 2006 American Chemical Society
Published on Web 01/27/2006

allowing the temperature depression at the surface to be estimated.

In a previous publication, we demonstrated that cavity-enhanced Raman scattering (CERS), can be used to probe the evaporation of multicomponent ethanol/water droplets, providing information on evolving droplet size and composition.[16] CERS occurs only at the discrete wavelengths commensurate with whispering gallery modes (WGMs), also commonly referred to as morphology dependent resonances (MDRs), providing a signature characteristic of droplet size.[32−34] Raman scattered light at WGM (MDR) wavelengths can remain trapped within the droplet for time scales of nanoseconds providing a mechanism for optical feedback which leads to stimulated Raman scattering.[35−37] A nonlinear signal that scales exponentially in amplitude with species concentration is observed.[38−40] As CERS is sensitive to the region of the droplet near the interface, the composition of a droplet can be quantified not only with high accuracy, but also with spatial selectivity.[41]

In addition to CERS providing information on particle size and composition, laser-induced fluorescence (LIF) can be used to probe the temperature of aerosol droplets, the pH of water droplets, and the efflorescence of inorganic aerosols.[27,42−45] In our previous work, we applied LIF to determine the volume-averaged droplet temperature of evaporating aerosol droplets containing ethanol and water and we extend the application of this technique in this work.[16]

In this publication, we exploit the CERS and LIF techniques for measuring the evaporation of a train of multicomponent alcohol/water droplets in the size range 23−57 μm in a dry nitrogen atmosphere over a pressure range 7−77 kPa. Gas diffusion limits the evaporative flux from the droplet under these conditions, which fall within the continuum regime.[46] The primary objectives of this study are to evaluate the effectiveness of quasi-steady state theory for examining the continuum regime evaporation dynamics of volatile droplets, to explore the possibility of measuring composition and temperature gradients in evaporating droplets, and to evaluate the experimental approach adopted. The experimental technique is briefly described in section 2 and the quasi-steady state theory in section 3.1.[31] In sections 3.2 and 3.3, we compare the experimentally measured evaporation rates and droplet temperatures with predictions made by quasi-steady state theory for the evaporation of multicomponent methanol/water, ethanol/water, and 1-propanol/water droplets and demonstrate that it is possible to extract vapor−liquid equilibrium data. We assess the signal volume probed by CERS in section 3.4 before some concluding remarks.

2. Experimental Technique

The CERS experimental technique for determining the composition of alcohol/water droplets has been described in previous publications, so only a brief account is presented here.[16,34,38,43] A monodisperse train of aerosol droplets is generated using a vibrating orifice aerosol generator (VOAG),[47] located within a regulated aerosol chamber. Alcohol/water droplets are produced by the VOAG in a continuously renewed dry nitrogen atmosphere at a pressure within the range 7−77 kPa. The droplet velocity is determined as 10 ± 1 m s^{-1} with a droplet separation distance estimated to be $\sim 6 \times 10^{-5}$ m. Both the stability and sphericity of individual droplets in the train are monitored by observing the elastic scattering diffraction pattern generated on illumination with a HeNe laser. This laser also serves to assist in aligning the droplet to the optical collection axis and the propagation axis of the probe Nd:YAG laser beam, operating at 355 nm. The probe laser beam is focused to a beam waist comparable to the droplet diameter, ensuring that only a single droplet in the aerosol train is illuminated. Laser pulse energies used in this work are typically 200 μJ, avoiding the optical saturation effects observed at higher energies.[39] The droplet train/aerosol chamber can be translated in two independent axes, along the laser beam and collection axes, allowing precise alignment.

The laser pulse, droplet generation and gating of the intensified CCD are synchronized to allow the CERS signal from a single droplet to be collected. Single laser pulse, single droplet CERS spectra are collected with a 0.5 m focal length spectrograph equipped with a 2400 g mm^{-1} diffraction grating, providing a wavelength dispersion of 0.012 nm/CCD pixel. Including the uncertainty in refractive index arising from changes in both droplet temperature and composition, droplet sizes are determined from CERS measurements with an accuracy of 0.1 μm.[16] Raman spectra are collected over a wavelength range 393−408 nm (Raman shift $\sim$2720−3660 cm^{-1}). This encompasses both the CH and OH Raman frequencies from the alcohol and water components. Composite CERS spectra were generated by the addition of $\sim$500 single droplet CERS spectra, allowing droplet composition to be determined by referencing the ratio of the integrated intensity of the CH to OH bands to a calibration plot.[16] This enables droplet composition to be determined with an estimated accuracy of $\pm$ 0.2% v/v.

The spectroscopic characterization of ethanol/water droplets has been investigated thoroughly in previous publications.[16,38,48] Here we extend this and present a spectroscopic characterization of both methanol/water and 1-propanol/water droplets, thus enabling subsequent studies of the dynamical response of these liquid droplets to their surrounding environment. We compare the spontaneous Raman spectra from bulk samples of 25% v/v methanol and 24% v/v 1-propanol collected using vertically polarized incident and scattered light in Figures 1 (a) and (b). All experimental parameters used were the same for both spontaneous and CERS measurements. The detailed spectral assignments for the bands are discussed elsewhere.[48−52] It is sufficient for our discussion here to identify the spectral range below a Raman shift of 3000 cm^{-1} as arising from the CH stretching vibrations of the alcohol, while the OH stretching Raman bands of liquid water and the alcohol appear above 3000 cm^{-1}. By examining Figure 1, it is apparent that only the most intense features in the CH stretching region of the spontaneous Raman spectra for the alcohols are sufficiently intense to rise above threshold for stimulated Raman scattering to occur. This leads to considerable simplification of the band structure on examining the CERS spectra.

In our previous publications, we have discussed, in detail, the compositional determination of ethanol/water droplets by CERS.[16,38] We demonstrated that the alcohol does not contribute to the OH CERS signature and the integrated CH and OH band intensities thus provide a direct measure of the alcohol to water composition ratio in the droplet. Following the procedures adopted in our earlier work, we have performed calibration measurements for the determination of droplet compositions for methanol/water and 1-propanol/water mixtures, which are independent of droplet size. The integrated CH and OH band intensities are compared with each other, and the variation in the ratio with composition is presented in Figure 2. The vapor pressures of ethanol and 1-propanol in the aqueous mixtures are sufficiently low at 298 K, estimated to be 1.85 and 1.6 kPa, respectively, that little evaporation occurs at the early times (0.2 ms) of the calibration measurements and at a gas pressure of 100 kPa.[16] However, the vapor pressure of methanol is 3.62

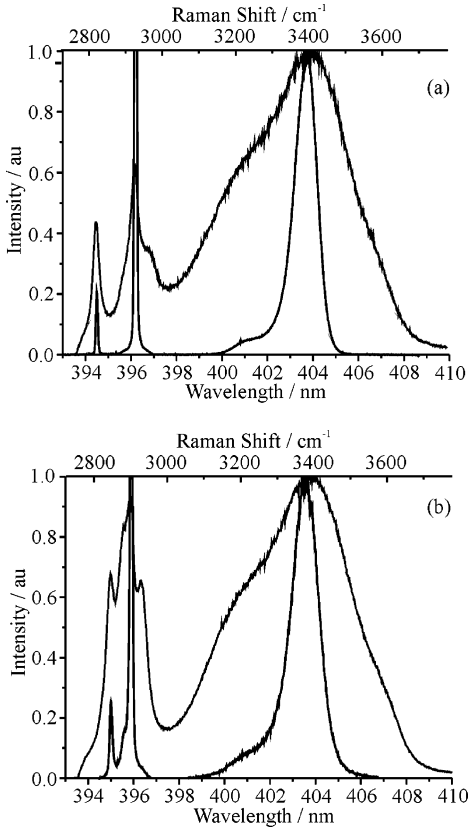

Figure 1. Comparison between bulk-phase spontaneous Raman spectra (black line) and droplet-stimulated Raman spectra (gray line) for compositions (a) 25% v/v methanol and (b) 25% v/v 1-propanol.

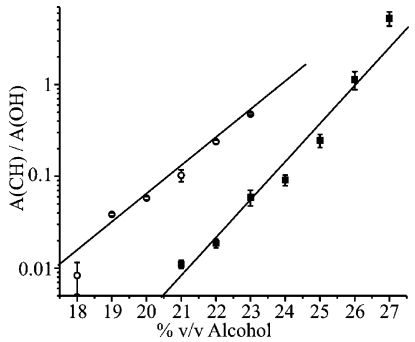

Figure 2. Calibration curves for the variation in the methanol and 1-propanol CERS integrated signal ratios for the OH and CH Raman stretches, *A*(*OH*) and *A*(*CH*), with change in composition for droplets 30.5 and 25 μm in radius, respectively. The filled squares and open circles represent the methanol and 1-propanol data, respectively.

kPa at 298 K. This leads to a small discrepancy between the prepared methanol concentration prior to droplet production and that measured by CERS, estimated to be 0.30 ± 15% v/v. This offset in calibration, although only slightly larger than the estimated error in compositional determination, is accounted for in the calibration curves used to analyze the evaporation data.

The limitations of using CERS to probe evaporation should be noted. Composition can only be determined over a narrow range. Thus, although CERS is ideal for probing the small changes in composition accompanying evaporation at an early time, the extensive changes in composition that are expected over a complete time history cannot be investigated. Further, during the early time period accessible to compositional measurements, the droplet radius does not change by more than the breadth of the size distribution of the droplets produced by the VOAG. Thus, droplet size changes during evaporation cannot be probed in the measurements described here.

Droplet temperature is characterized using LIF with laser excitation at 355 nm and with all experimental parameters the same as for the CERS measurements.[16,27,42] The only difference is that pulse energies of <100 μJ/pulse were used in order to avoid the stimulated emission at WGM wavelengths that result at higher pulse energies. In previous work using pH sensitive dyes, we have demonstrated that at such low irradiances, the fluorescence profile conforms to that observed in bulk phase measurements.[43] In this case, this allows an unambiguous comparison with bulk calibration measurements to be employed for temperature determination. Multicomponent alcohol/water droplets are doped with the temperature sensitive dye rhodamine B at a concentration of 1×10^{-6} M. LIF from droplets is collected using a 300 g mm^{-1} diffraction grating, which provides a wavelength dispersion of 0.096 nm/CCD pixel. Spectra are accumulated from 500 droplets, collected over a wavelength range 520−680 nm, and compared to a bulk phase calibration enabling the determination of droplet temperature with an associated error estimated to be better than ± 1 K.[16]

3. Results and Discussion

The mass transfer accompanying evaporation from a droplet surface requires heat transfer from the gas phase to maintain a constant rate of evaporation.[46,53,54] For volatile components, such as the water and alcohol components in the current study evaporating into a dry nitrogen atmosphere at reduced pressures, heat transfer from the surrounding gas is not sufficiently rapid to maintain the droplet surface temperature at its initial value.[30,54] During this unsteady period, the droplet cools, leading to a lowering of the vapor pressure of the droplet constituents at the droplet surface and a corresponding decrease in the rate of mass transfer.[55] After this transient period, a limiting steady state is reached, characterized by evaporation at a constant droplet temperature at which the heat flux to the droplet from the gas-phase balances the heat lost due to evaporation, the droplet temperature is steady, and the mass transfer rate is constant.[25] Maxwell was the first to solve the steady-state conservation equations of mass and energy in the gas phase for the evaporation into a stagnant gas in order to explain the phenomenon of the wet-bulb temperature.[53,56] This derivation assumes that equilibrium is established for the gas and liquid at the interface and that convection effects are negligible.

In a preliminary investigation of the evolving composition of evaporating ethanol/water droplets, we have shown that a steady state treatment fails to accurately predict the vapor pressures of the droplet constituents.[16] Steady state theory is only appropriate for isothermal evaporation, for which the vapor pressures of the components are approximately constant. The rate of mass transfer is independent of time and determined by the concentration gradient of the evaporating component from the droplet surface to an "infinite" distance, the diffusion constant of the evaporating component in the gas phase, and the droplet surface-to-volume ratio. By contrast, nonisothermal behavior is observed for the rapid evaporation of highly volatile components, as in the systems studied here, and the temperature depression of the surface must be explicitly included in the heat and mass transfer analysis to account for the time-dependent evaporation rate.[25,26,30,54] Although a full unsteady treatment would be desirable, quasi-steady state theory provides a good compromise between the steady and unsteady-state approaches.[1,29,31,53,55] A better description of the physical processes occurring than steady state theory is achieved while reducing

the complexity of the unsteady state model. We first introduce the quasi-steady state theory and apply it to studies of the evaporation of ethanol/water and methanol/water droplets. We then note some discrepancies that arise between prediction and experiment for the evaporation of 1-propanol/water droplets, and, finally, we consider the region of the droplet probed by the CERS measurements.

3.1. Quasi-Steady-State Evaporation Theory. A quasi-steady treatment of droplet evaporation considers that, at any particular instant in time, the concentration and temperature profiles in the gas-phase surrounding the particle, and the mass and energy fluxes, can be treated as if they were in steady state.[29,55] Any changes in concentration or temperature profile or flux can be expressed as arising from a change in the boundary conditions at the droplet surface or at a large distance from the droplet. This can be assumed to be a good approximation if the time for establishing a stable concentration or temperature profile in the surrounding gas phase is much shorter than the time scale over which the physical state of the system (droplet radius, temperature, and composition) is changing.[1,55]

Newbold and Amundson derived a quasi-steady model for the evaporation of a multicomponent droplet in a stagnant gas.[31] The model describes the transport of n vapors through an inert gas around a single isolated and stationary aerosol droplet. The transport equations for the gas-phase are first solved, thus generating expressions for the mass flux and heat flux from the droplet. Differential equations describing the change in droplet radius, concentration, and temperature with time are then derived from considering the mass, volume, and energy balances expressed in terms of the mass and heat fluxes. The droplet surface and the boundary conditions are assumed to change slowly with time, allowing the evaporation to be treated within the quasi-steady approximation. In addition, the gas−liquid interface is assumed to be at equilibrium, which inherently means that the interfacial transfer between the liquid and gas phases is rapid compared to gas-diffusion away from the droplet. This is a valid assumption for the systems considered here which all fall within the continuum regime. The mean free path of the gas-phase molecules, λ, is much shorter at the pressures presented in this work than the droplet radius, R_p, and the Knudsen number, Kn, defined as

$$Kn = \frac{\lambda}{R_p} \tag{1}$$

is considerably less than 1. Knudsen numbers calculated from the range of pressures (7−77 kPa) and droplet sizes (23−57 μm) used in this work fall within the range 4×10^{-2} and 2×10^{-3}; thus, evaporation is limited by gas diffusion.

To assess the validity of the quasi-steady treatment, Seinfeld and Pandis demonstrate that the time scale for gas-phase diffusion to establish a steady-state concentration profile of a species around the particle, τ_{gd}, can be estimated from the gas diffusion constant for the species, D_g, and the droplet radius, R_p:[1]

$$\tau_{gd} = \frac{{R_p}^2}{4D_g} \tag{2}$$

The diffusion constant spans the range 1.5×10^{-5} m^2 s^{-1} at 100 kPa to 1.5×10^{-4} m^2 s^{-1} at 10 kPa for ethanol diffusing in dry nitrogen. For the smallest droplets of 23 μm radius studied in this work at the lowest pressure, τ_{gd} can be as short as 0.9 μs. Thus, for the smallest droplets, which evaporate and cool most rapidly, the gas phase compositional profile around the droplet responds to changes at the particle surface very rapidly, and the use of quasi-steady model can be justified. For the largest droplets of ~55 μm radius at the highest pressure, the time scale for gas-phase diffusion to establish a steady-state concentration profile of a species around the particle is $\tau_{gd} \sim$ 50 μs. Although the application of the quasi-steady approximation might be questionable for probing droplets at the early time investigated in this work (200 μs) with such a slow gas phase response time, changes in droplet size, composition, and temperature can also be expected to be very slow for such large droplets, and the quasi-steady approximation can be similarly justified.

The equations essential for defining the mass and heat transfer problem and for modeling the experimental data are summarized below. The equations define the change in droplet radius, composition, and temperature with time, t, for a multicomponent droplet composed of n species evaporating into a gas composed of n volatile components and an inert gas ($n + 1$ components in total). A full derivation of these equations is found in reference 31. Radial convection, also referred to as Stefan flow, is directly accounted for.[31] Stefan flow must be included when the partial pressure of the evaporating component at the droplet surface is large compared to the total gas pressure surrounding the droplet.

The mass (eq 3) and energy (eq 4) fluxes as they depend on the radial coordinate r can be described by the equations

$$\frac{dy_i}{dr} = \sum_{j=1}^{n+1} \frac{1}{C_T D_{ij}} (y_i N_j - y_j N_i) \tag{3}$$

and

$$e = -k\frac{dT}{dr} + \sum_{j=1}^{n+1} N_i H_i \tag{4}$$

where the former of these two equations is the Stefan−Maxwell equation. The net molar flux of component i is given by N_i and is a function of r. The total energy flux, also a function of r, is given by e. The radial dependence of the mole fraction of component i in the gas phase is given by y_i. The total gas concentration at temperature T is given by C_T, and D_{ij} is the binary diffusivity of gas i with respect to gas j. The molar enthalpy of the ith component of the gas is given by H_i. In determining the energy flux, the Dufour effect (diffusion−thermo effect) has been neglected, omitting the dependence of the energy flux arising from the diffusing species. Similarly, the dependence of the mass flux on the temperature gradient, the Soret effect (thermal−diffusion effect), has been neglected.

Two assumptions must be made to determine the molar flux of component i from the droplet surface, N_{i,R_p}, eq 3: the binary diffusivities are replaced by an effective binary diffusivity of component i with respect to the mixture, D_{im}; and the quasi-steady approximation is made. This leads to the following expression:

$$N_{i,R_p} = \frac{C_T D_{\mathrm{Im}}}{R_p p} \ln(\chi) \left[\frac{x_i p_i^0(T_{R_p}) \chi^{D_{\mathrm{Im}}/D_{im}} - p_{i,\infty}}{\chi^{D_{Im}/D_{im}} - 1} \right] \tag{5}$$

where the subscript I refers to the inert gas which does not transfer across the surface and D_{Im} is the diffusion coefficient of the inert gas in the mixture. x_i is the mole fraction of the ith component in the droplet and $p_i^0(T_{R_p})$ is the vapor pressure of

pure component i at the droplet surface temperature. p is the total gas pressure, and $p_{i,\infty}$ is the partial pressure of component i at an infinite distance from the droplet, which can be assumed to be zero for each of the volatile components in these measurements as evaporation is into a constantly refreshed dry nitrogen atmosphere. Finally, χ is defined as

$$\chi = \frac{y_{\mathrm{I},\infty}}{y_{\mathrm{I},R_p}} = (1 - \sum_{i=1}^{n} y_{i,R_p})^{-1} \quad (6)$$

and is the ratio of the inert gas composition in the bulk gas, $y_{\mathrm{I},\infty}$, to that at the interface, y_{I,R_p}.

If there is no thermal expansion and no volume change due to mixing then the volume change of the droplet corresponds to the volume of liquid vaporized. The rate of change of droplet volume can be expressed as

$$\frac{dV_d}{dt} = -4\pi R_p^2 \sum_{i=1}^{n} N_{i,R_p} V_i \quad (7)$$

where V_i is the molar volume of species i. This equation can be used to derive the rate of change of droplet radius with time,

$$\frac{dR_p}{dt} = -\sum_{i=1}^{n} N_{i,R_p} V_i \quad (8)$$

From considering the mass balance on component i, the rate of change of the mole fraction of component i in the droplet is given by

$$\frac{dx_i}{dt} = \frac{3V_m}{R_p} \sum_{j=1}^{n} N_{j,R_p} \left(x_i - \frac{N_{i,R_p}}{\sum_{j=1}^{n} N_{j,R_p}} \right) \quad (9)$$

where V_m is the mean molar volume defined as $V_m = \sum_{i=1}^{n} x_i V_i$.

The energy balance, ignoring radiation effects, can be used to derive an expression for the change in the temperature of the droplet with time:

$$\frac{dT_{R_p}}{dt} = \frac{3V_m}{R_p C_{p,m}} \left\{ \frac{\kappa_2 A}{(e^A - 1)R_p} (T_\infty - T_{R_p}) - \sum_{i=1}^{n} N_{i,R_p} [\Delta H^0_{i,vap} + \Delta C_{p,i}(T_{R_p} - T_0)] \right\} \quad (10)$$

where $C_{p,m}$ is the heat capacity of the mixture and κ_2 is the gas thermal conductivity. A is defined as

$$A = \frac{R_p}{\kappa_2} \sum_{i=1}^{n} N_{i,R_p} C_{p,i} \quad (11)$$

T_∞ is the temperature at an infinite distance from the droplet, T_{R_p} is the temperature at the droplet surface and T_0 is the initial droplet temperature. $\Delta C_{p,i}$ is the difference in molar heat capacities of the ith component for gas and liquid phases. $\Delta H^0_{i,vap}$ is the enthalpy of vaporization for the ith component of the liquid.

Equations 8, 9, and 10 form the basis for describing the evolution in the radius, composition and surface temperature of the multicomponent droplet with time. Having now defined all of the constants required for the model, the constants for each of the three systems described are reported in Table 1.

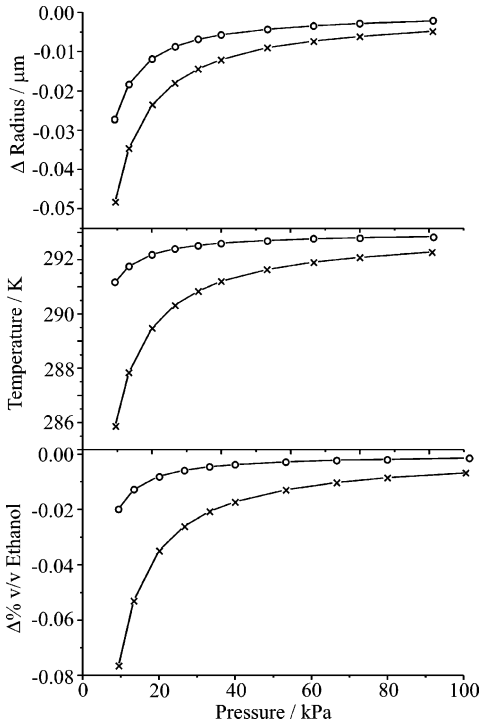

Figure 3. Quasi-steady state theoretical calculations illustrating the variation in droplet temperature, change in droplet size and composition with change in the surrounding dry nitrogen gas pressure at an evaporation time of 0.2 ms. Droplets are initially composed of 18.4% v/v ethanol with an initial radius of 26 and 57 μm, crosses and open circles, respectively.

TABLE 1: Constants Used in the Quasi-steady State Model Simulations

	18.6% v/v m^{-1} mol^{-1} ethanol	25% v/v m^{-1} mol^{-1} methanol	24% v/v m^{-1} mol^{-1} 1-propanol
molar volume of water[60]	1.80×10^{-5}	1.80×10^{-5}	1.80×10^{-5}
molar volume of alcohol[60]	5.83×10^{-5}	4.04×10^{-5}	7.47×10^{-5}
$D_{Alc,N2}$/atm cm^2 s^{-1}[63]	0.147	0.176	0.129
D_{H_2O},N_2/atm cm^2 s^{-1}[63]	0.259	0.259	0.259
D_{N_2},N_2/atm cm^2 s^{-1}[63]	0.24	0.24	0.24
C_{P,N_2}/J mol^{-1} K^{-1} (300 K)[60]	29.125	29.125	29.125
C_{P,H_2O}, l/J mol^{-1} K^{-1} (298 K)[60]	75.29	75.29	75.29
C_{P,H_2O}, g/J mol^{-1} K^{-1} (298 K)[60]	33.58	33.58	33.58
κ_{N_2}/W m^{-1} K (300 K)[60]	25.8×10^{-3}	25.8×10^{-3}	25.8×10^{-3}
$C_{P,Alc,l}$/J mol^{-1} K^{-1} (298 K)[60]	111.46	81.11	144.44
$C_{P,Alc,g}$/J mol^{-1} K^{-1} (298 K)[60]	65.44	44.06	85.56
$\Delta H_{vap,H_2O}$/J mol^{-1} K (298 K)[60]	43.98×10^3	43.98×10^3	43.98×10^3
$\Delta H_{vap,Alc}$/J mol^{-1} K (298 K)[60]	42.32×10^3	37.43×10^3	47.45×10^3
V_{p,H_2O}/Pa (280 K)[60]	1000	1000	1000
$V_{p,Alc}$/Pa (302 K)[60]	10 000	20 600	3600
γ_{Alc}[58,59]	1.54	1.45	7.9
γ_{H_2O}[58,59]	0.93	1.02	1.04

The equations were integrated using a fourth order Runge−Kutta routine using a variable step size enabling this series of equations to be solved numerically. Figure 3 illustrates the calculated influence of the inert buffer gas pressure on the composition, size, and temperature of droplets initially 26 and 57 μm in radius, composed of 18.4% ethanol at an evaporation time of 0.2 ms. In these predictions, a change in the gas pressure leads not only to a change in the rate of mass transfer but also the rate of heat transfer, i.e., the effective binary diffusivity of each component, the total concentration of molecules in the gas phase, and the mole fractions of each of the components at the droplet surface all change. With increasing gas pressure, the rate of mass loss and the rate of surface cooling are both predicted to decrease. This will serve as an example of what should be expected in the experimental studies which follow.

The derivation of the mass, volume and energy balances assume the temperature and concentrations are uniform over the volume of the droplet. Considering the temperature to be uniform can be justified for most gas−liquid systems because the liquid thermal conductivity is considerably greater than the gas thermal conductivity.[55] The heat lost from the droplet over a certain time period is assumed to be removed from the entire droplet volume and not just from the surface and the quasi-steady treatment yields a surface temperature that is also the temperature throughout the droplet. Assuming that the composition is uniform throughout the droplet, however, implies that liquid phase diffusion must be rapid compared to evaporation or very much slower. This condition is rarely fully satisfied, and may lead to higher than expected evaporation rates for some components and lower rates for others.[31] In an analogous way to temperature, the quasi-steady treatment yields a droplet composition that is spatially uniform, but reflects the mass loss of each component from the droplet surface as arising from the entire droplet volume.

Part of the impetus for developing the techniques described here is to examine the spatial inhomogeneities in droplet composition and temperature that arise during heat and mass transport. For the large droplets considered in this work (>23 μm radius) and the slow rate of liquid phase diffusion, gradients in composition within the droplet are to be expected. An ethanol molecule can be estimated to diffuse only ~0.6 μm on the 0.2 ms time scale of the experiments presented here.[16] Similarly, the size of the droplet is likely to lead to temperature inhomogeneities within the droplet.[57] The composition measurements probe the near-surface composition and, thus, are expected to show a greater depletion of ethanol than is calculated from the quasi-steady model. That thermal conduction also occurs on a finite time scale is also likely to lead to a volume averaged temperature measured by LIF that will be higher than that predicted from quasi-steady theory in which the heat lost from the droplet is averaged instantaneously over the entire droplet volume. Such gradients in composition and temperature within the droplet will be reflected in differences between the absolute measured and calculated droplet compositions and temperatures. However, the rates of heat and mass transfer within the droplet, limited by thermal conduction and diffusion, are expected to be approximately constant for all of the droplet sizes and for all of the pressure dependent measurements presented here. Thus, the composition and temperature changes predicted by the quasi-steady model should still provide an analysis of the total mass and heat flux from an evaporating droplet, and correlations between the calculated and measured compositions and temperatures for a range of droplet sizes and pressures might be expected.

3.2. The Evaporation of Ethanol/Water and Methanol/Water Binary Droplets. In our earlier work, we demonstrated that the evolving composition of evaporating ethanol/water droplets of a particular initial radius could be interrogated as a function of time or as a function of inert buffer gas pressure.[16] In this study, we present a more thorough investigation of the dependence of change in droplet composition and temperature on the dry nitrogen gas pressure at a fixed evaporation time of 0.2 ms. The concentration of alcohol remaining in the droplet after this time provides a measure of the relative fluxes of alcohol and water away from the droplet. We have performed this investigation for three alcohol/water systems (18.4% v/v ethanol, 25% v/v methanol, and 24% v/v 1-propanol) and for a range of initial droplet sizes; we have used these data to rigorously test the quasi-steady model described above by examining correlations between the measured and predicted compositions and temperatures.

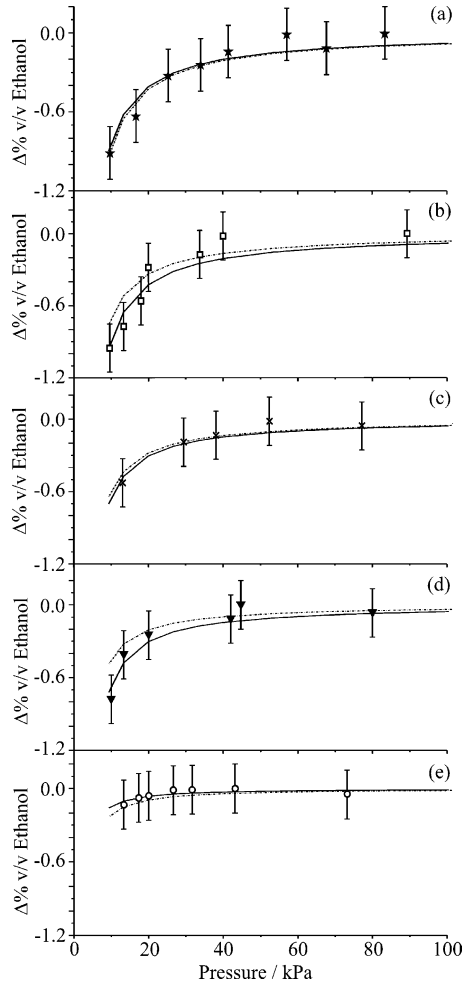

Figure 4. Variation in ethanol concentration with nitrogen gas pressure probed at 0.2 ms for droplets of radius (a) 26, (b) 29, (c) 32, (d) 37.8, and (e) 57 μm. In each figure, the solid line represents the quasi-steady state prediction scaled by factors of 12.3, 14.8, 12.8, 17.3, and 7.9, respectively. The dashed line represents the quasi-steady-state model using a scaling factor of 11.4 in each case.

We first describe the experimental measurements and theoretical predictions for the dependence of the final ethanol concentration on gas pressure for five droplet sizes; these data are presented in Figure 4. It is evident that the evaporative flux of ethanol from the droplet increases on reducing the pressure of dry nitrogen surrounding the droplet due to the increased gas diffusion rate. A higher evaporative flux is experienced by the smallest droplets compared to the largest droplets. This is a consequence of the change in surface area-to-volume ratio which is a factor of ~2.2 larger for the 26 μm radius droplets compared to droplets 57 μm in radius.

The general trends observed are comparable to those predicted by quasi-steady state theory and shown in Figure 3. Activity coefficients of 1.54 for ethanol and 0.93 for water are used in the quasi-steady-state model to account for the positive deviation from Raoult's law which occurs for this 18.4% v/v ethanol system.[58] As discussed earlier, the change in % v/v alcohol predicted by the model is assumed to be uniform over the whole droplet and this is considerably less than that measured experimentally by CERS near the surface. This suggests the existence of composition gradients within the evaporating droplet as anticipated. The CERS measurement determines the change in % v/v alcohol occurring in the outer shell of the

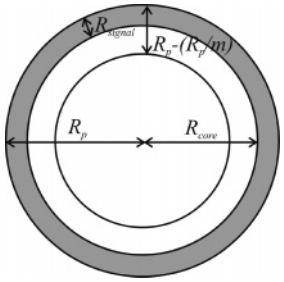

Figure 5. Schematic showing the estimated CERS signal volume (shaded gray) of shell thickness R_{signal} as a fraction of the total droplet volume. The maximum distance to which whispering gallery modes can propagate is also highlighted, $R_p-(R_p/m)$.

droplet, from the interface to a depth of $R_p - (R_p/m)$ from the interface, as illustrated in Figure 5, where m is the refractive index of the droplet medium.[16] This reflects the maximum distance from the interface that the circulating light can penetrate while still approaching the surface at an angle greater than the critical angle required for total internal reflection to be maintained.[32] We consider a simple single parameter scaling of the prediction to the experimental data to reconcile the quasi-steady model to the experimental data, thus allowing a comparison of the qualitative trends observed and predicted.

The scaling factors applied to the model which provide the best fit to the experimental data for each initial droplet size are presented in Figure 4, and they are determined by examining the mean square deviation of the scaled model prediction from the experimental results. These scaling factors show no systematic dependence on droplet size and are 12.3, 14.8, 12.8, 17.3, and 7.9 for droplets of radius 26, 29, 32, 37.8, and 57 μm, respectively. The independence of the scaling factor from size is expected as the signal volume for a given droplet refractive index is a constant fraction of the entire droplet volume, W(signal). Thus a constant scaling should be anticipated, i.e.,

$$W(\text{Signal}) = \frac{R_p^3 - (R_p/m)^3}{R_p^3} = 1 - (1/m)^3 = 0.589 \quad (12)$$

Thus, the best-fit scaling factor for all of the droplet sizes studied for this ethanol/water system can be calculated as 13 ± 3.5, reducing the comparison between the model and all of the data to a single scaling factor.

The pressure dependencies for the evaporation of 25% v/v methanol/water droplets starting at five different initial droplet radii are shown in Figure 6. It should be noted that the depletion of methanol from the droplet at the lowest gas pressure is higher than that for ethanol under the same conditions, and this is consistent with the higher vapor pressure of the alcohol in the methanol/water mixture compared to the ethanol/water mixture. The best-fit scaling of the quasi-steady-state model predictions are compared to pressure dependent experimental evaporation data, using activity coefficients of 1.45 for methanol and 1.02 for water, which account for the positive deviation of the vapor pressure from Raoult's law.[59] Scaling factors which provide the best fit to the experimental data have been determined as 9.8, 10.5, 10.4, 8.0, and 11.7 for droplets of radius 23, 27, 30.5, 35, and 57 μm, respectively. Once again, there is no systematic dependence on droplet size and a mean scaling factor of 9.7 ± 1.7 for the methanol/water system can be estimated.

The mean scaling factors for both the ethanol and methanol experiments are within one standard deviation. Indeed, the use of only one scaling factor is considered appropriate for the

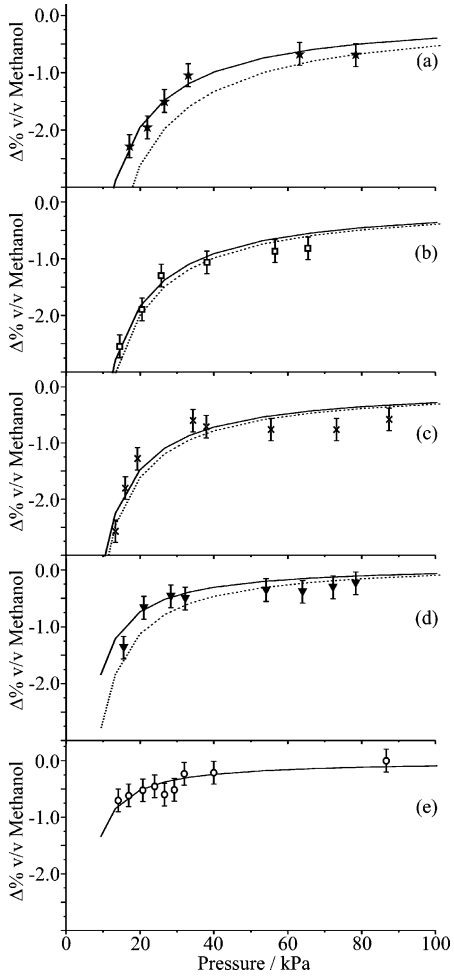

Figure 6. Variation in methanol concentration with nitrogen gas pressure probed at 0.2 ms for droplets of radius (a) 23, (b) 27, (c) 30.5, (d) 35, and (e) 57 μm. In each figure, the solid line represents the quasi-steady state prediction scaled by factors of 9.8, 10.5, 10.4, 8.0, and 11.7, respectively. The dashed line represents the quasi-steady-state model using a scaling factor of 11.4 in each case.

combined data set for all of the data from the 18.4% v/v ethanol and 25% v/v methanol systems, and this can be justified as follows. The difference in refractive index between the 18.4% v/v ethanol and 25% v/v methanol systems studied in this work is minimal, 1.3455 compared to 1.3392,[60] respectively. Thus, the signal volume as a fraction of the total droplet volume, calculated from eq 12, is comparable for the two systems (0.589 and 0.584 for the ethanol and methanol systems, respectively) and, thus, a similar scaling factor should be expected. The mean scaling factor for the combined ethanol/water and methanol/water systems is equal to 11.4 ± 3, and the level of quantitative agreement between the quasi-steady model and all of the data for both the ethanol and methanol systems, as shown in Figures 4 and 6, remains high.

Thus, we can conclude that the compositional changes determined experimentally for both the ethanol and methanol systems are broadly consistent with the predictions of the quasi-steady model. However, the required scaling factor for the model to compare with the measurements demonstrates that the compositional change occurs within the outer shell on the time scale of these measurements, and a compositional gradient is formed. In further support of this conclusion, we have examined the correlation between calculated surface temperature and measured temperature during the first 10 ms of evaporation for a range of initial droplet sizes. At this point it is helpful to

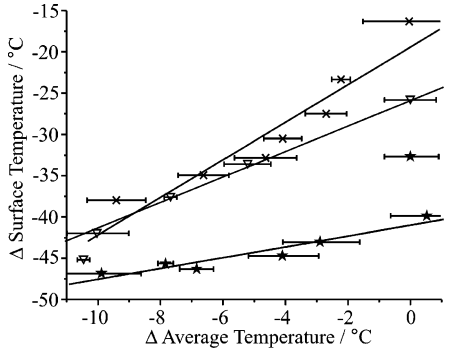

Figure 7. Correlation between the average and surface temperature for droplets initially composed of 25% v/v methanol with radius 25, 35, and 57 μm (stars, triangles and crosses, respectively), measured with evolving time, 0.2−10 ms. The lines represent fits to the data.

reiterate that, when we refer to the experimentally determined temperature, the LIF technique probes the volume averaged temperature of the droplet; the fluorescence spectrum recorded is a convolution of signal originating from all parts of the droplet with the core of the droplet responding only slowly to changes in temperature at the droplet surface. This should be contrasted with the quasi-steady-state model which predicts the surface temperature of the droplet and which is assumed to be uniform throughout the droplet. A clear correlation is observed and is shown in Figure 7 for three different droplet radii (25, 35, and 57 μm), initially composed of 25% v/v methanol, evaporating into a dry nitrogen atmosphere maintained at 7 kPa. The smallest droplets experience the greatest evaporative cooling in this time period, and this is, again, consistent with the quasi-steady model predictions. As for the compositional measurements, the difference between the measured and predicted temperatures reflects the existence of temperature gradients within an evaporating droplet.

3.3. Evaporation of Multicomponent 1-Propanol/Water Droplets. Experiments similar to those described above have been conducted for droplets composed of 1-propanol/water with initial radii of 23, 31, 37.8, and 57 μm. These data are shown in Figure 8. It is expected that the radial extent from which WGMs penetrate in the 1-propanol/water system is not too dissimilar from that determined for the ethanol/water and methanol/water systems. Thus, the signal volume as a fraction of the total droplet volume will be similar. Once again using eq 12, the signal volume fraction can be calculated to be 0.597 taking the refractive index of a 24% v/v 1-propanol as 1.3539, which compares favorably to the ratios of 0.589 and 0.584 calculated for the ethanol and methanol systems, respectively.[60] Therefore, it is reasonable to assume that the same scaling factor of 11.4 ± 3 must be applied to bring the quasi-steady state prediction into line with the experimental data. Activity coefficients of 7.9 for 1-propanol and 1.04 for water were used in the model to account for the positive deviation in the vapor pressure from Raoult's law which occurs for the 24% v/v 1-propanol system.[59] As is evident in Figure 8, the scaled model clearly over predicts the evaporative flux from the 24% v/v 1-propanol droplets when compared to the experimental data. A scaling factor of ~2 must be applied to the quasi-steady state prediction to give a satisfactory fit to the experimental data, rather than the factor of 11.4. Indeed, the quasi-steady state model predicts a faster evaporation rate for 24% v/v 1-propanol than is predicted for 18.4% v/v ethanol. Irrespective of the model scaling, the opposite trend is observed experimentally and the alcohol is observed to evaporate at a higher rate from 18.4% v/v ethanol droplets than 24% v/v 1-propanol droplets.

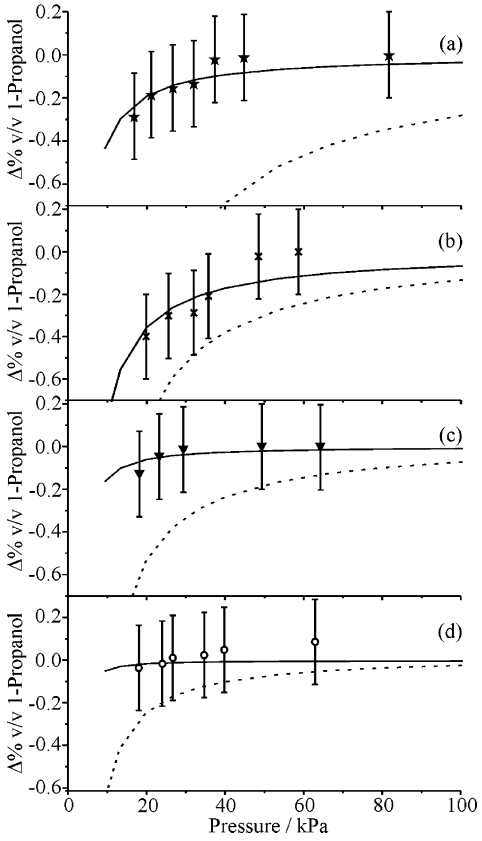

Figure 8. Variation in 1-propanol concentration with nitrogen gas pressure probed at 0.2 ms for droplets of radius (a) 23, (b) 31, (c) 37.8, and (d) 57 μm. The solid lines represent the quasi-steady state prediction scaled by a factor of 11.4 using activity coefficients for 1-propanol of 3, 4.8, 2.9, and 2.5, respectively. The dashed line represents the quasi-steady-state model using a scaling factor of 11.4 in each case.

Having examined the mass transfer rate for evaporating 1-propanol/water droplets and observed a lower evaporation rate than is expected, it is instructive to examine the heat transfer that occurs by investigating the change in temperature of the droplet. We have performed LIF measurements for all three aqueous/alcohol systems, examining the temporal variation in droplet temperature at the lowest dry nitrogen pressure of 7 kPa and for droplets initially ~40.2 μm in radius. The data are presented in Figure 9. It is evident that the greatest cooling is observed for the 25% v/v methanol system with the smallest cooling occurring for the 24% v/v 1-propanol system. The cooling observed for the 18.4% v/v ethanol system lies between these two extremes. This qualitative trend can be rationalized by considering the vapor pressures of the alcohol/water solutions (3.62, 1.85, and 1.6 kPa at 298 K for methanol, ethanol, and 1-propanol, respectively) and the resulting relative mass transfer rates.[58−60] However, the magnitudes of the temperature changes accompanying the evaporation must be considered. A decrease in the average droplet temperature of ~11 ± 1 °C is measured for the 25% v/v methanol system at a time ~5 ms after generation with a slower rate of temperature decrease measured at longer times. The same effect is observed for the droplets composed of 18.6% v/v ethanol, with a maximum temperature depression of ~8 ± 1 °C observed. The temperature depression of 24% v/v 1-propanol is negligible over the time scale of the measurements, and little change is observable when the error bars are considered.

Using the quasi-steady-state model, the droplet surface temperature change has been estimated for all three systems, and the model predictions are shown in Figure 9(b). A surface

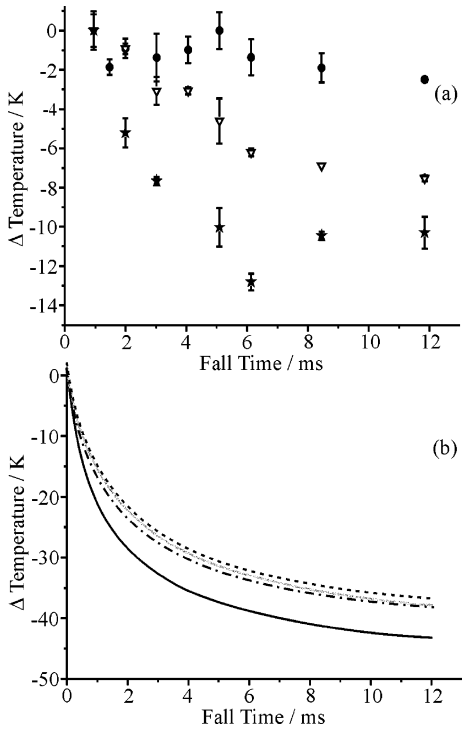

Figure 9. (a) Measurements of the evaporative cooling of 25% v/v methanol, 18.6% v/v ethanol and 24% v/v 1-propanol droplets (stars, triangles, and circles, respectively) probed by LIF. (b) Predicted surface temperature depression of 25% v/v methanol ($\gamma = 1.45$), 18.6% v/v ethanol ($\gamma = 1.54$), and 25% v/v 1-propanol ($\gamma = 3.3$ and $\gamma = 7.9$) droplets, black solid line, gray solid line, black dashed line, and black dot dashed lines, respectively. Droplets are initially ~40.2 μm in radius and measurements are conducted at a dry nitrogen pressure of 7 kPa.

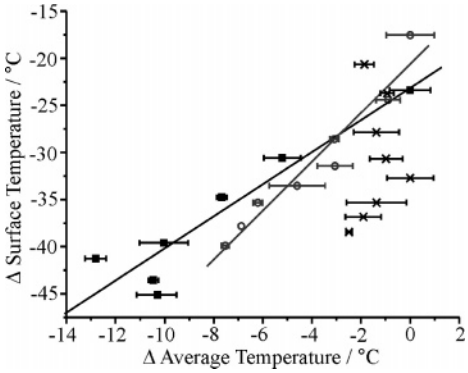

Figure 10. Correlation between the average and surface temperature for droplets initially composed of 25% v/v methanol, 18.6% v/v ethanol, and 24% v/v 1-propanol droplets (stars, triangles, and circles, respectively) at the lowest dry nitrogen pressure of 7 kPa and for droplets initially ~40.2 μm in radius. The lines represent fits to the data.

temperature depression of ~40 K for the methanol/water system is predicted at a time of 5 ms, considerably larger that the average droplet temperature depression measured using LIF. Comparable surface temperature depressions are predicted for the ethanol/water and 1-propanol/water systems, with predicted surface temperature decreases of 33 and 34 K, respectively. This is in contrast to the measured temperatures which show no temperature depression for the 1-propanol system.

The poor correlation between the predicted surface temperature and measured volume averaged temperature for the 1-propanol system is markedly apparent if we compare the correlations between the two for all three alcohol systems (Figure 10) for the time dependent data shown in Figure 9. Similar linear correlations are observed between the surface and average droplet temperatures for the methanol and ethanol systems, showing that the experimental data is broadly consistent with the quasi-steady model, in agreement with the trends observed for the size-dependent measurements of Figure 7, although a temperature gradient does exist within the droplet. However, the mild depression of temperature measured for the 1-propanol system leads to a poor correlation to the model for this system. This, along with the discrepancy observed in the compositional data, supports the conclusion that the model fails to capture all of the required detail occurring during evaporation for this system.

The reason for the poor correlation between the quasi-steady predictions and the experimental measurements for the 1-propanol system is not immediately clear. However, a number of possible factors can be discussed that may account for this difference and these may serve as pointers for further experimental work. Nathanson and co-workers have demonstrated that the presence of a butanol film on the surface of sulfuric acid does not impede the evaporation of water from a liquid surface and so it is unlikely that the discrepancy in the measured and calculated mass transfer rates arises from a kinetic effect occurring as a result of a surface excess of the alcohol inhibiting evaporation.[61,62]

The thermal conductivities for liquid water, methanol, ethanol, and 1-propanol are 0.606, 0.202, 0.167, and 0.154 W/m K, respectively, compared with the value of 0.0258 W/mK for gas-phase nitrogen at 25 °C.[60] The substantially larger values for the liquid compared with the gas form the basis for the assumption made in the quasi-steady model that the temperature is uniform throughout the droplet. However, it is noticeable that the thermal conductivity for 1-propanol is the lowest of the three alcohols, suggesting that a temperature gradient between the surface and the core may be largest for this system. This could be identified as an example of the type of system for which the internal temperature gradient leads to an overestimate by the quasi-steady model of the mass flux from the droplet. This is broadly consistent with the LIF measurements, and could result in a much lower evaporation rate from the droplet than is predicted with the surface undergoing more rapid cooling than is predicted. However, it should also be noted that the dominant component in these droplets is water, and its thermal conductivity is considerably larger than that of the alcohols. In addition, the thermal conductivity of 1-propanol is <10% different from that of ethanol.

A possible but unlikely source of error which could contribute to the discrepancy between the model output and the experimental results is the activity coefficient of 1-propanol (γ_{PrOH}). On investigation, an error in the activity coefficient of 1-propanol has a significant impact on the model's prediction. If the equilibrium value of γ_{PrOH} is considered to be in error and the scaling factor of 11.4 ± 3 is assumed to be valid for the 1-propanol/water data as well as for the other alcohol systems, it is possible to determine the value of γ_{PrOH} which would give the best theoretical fit to the experimental data. The lowest mean square deviation of the scaled model from the experimental data represents the best fit to the experimental data. This yields values for γ_{PrOH} of 3 ± 0.3, 4.8 ± 0.5, 2.9 ± 0.3, and 2.5 ± 0.3 for measurements made on droplets of radius 23, 31, 37.8, and 57 μm, respectively. An overall mean value of $\gamma_{PrOH} = 3.3 \pm 1$ is obtained from these results, a factor of 2.4 lower than the value of 7.9 measured by Butler et al.[59] Figure 8 presents the experimental data sets for the four droplet sizes studied in this work compared to the best fit to each individual data set. However, it should also be noted that although this leads to a

surface temperature depression that is now smaller in magnitude than that predicted for the ethanol system, the correlation between the surface temperature prediction and the measurements remains poor, as seen in Figure 9.

3.4. Estimating the Signal Volume. As stated previously, the scaling factor applied to the quasi-steady state prediction to bring it into agreement with the experimental results can be used to estimate R_{signal}. The scaling factor, S, of 11.4 ± 3 determined from the combined ethanol/water and methanol/water data is used in this analysis. It is important to note that this scaling factor is considerably larger than the factor of 1.7 that is predicted from eq 12, suggesting that the signal is much more sensitive to the near-surface region than is initially expected. With knowledge of the quasi-steady-state forecast of % v/v alcohol for the whole droplet, $\%\ V^f_{Alc,Quasi}$, the initial % v/v alcohol, $\%V^i_{Alc}$, and the scaled model prediction which represents the % v/v alcohol in the outer shell of the droplet, $S\%V^f_{Alc,Quasi}$, the penetration depth of the signal can be estimated by referring to Figure 5. The forecast of % v/v alcohol for the whole droplet is given by:

$$\%\ V^f_{Alc,Quasi} = \frac{V_{signal}}{V_{total}}(\%V^i_{Alc} - S\Delta\%V^f_{Alc,Quasi}) + \frac{V_{core}}{V_{total}}\%V^i_{Alc} \quad (13)$$

where $V_{total} = {}^4/_3\pi R_p^3$, $V_{core} = {}^4/_3\pi R_{core}^3$ and $V_{signal} = V_{total} - V_{core}$. This assumes no depletion occurs in the droplet core. Equation 13 can now be simplified to

$$\%\ V^f_{Alc,Quasi}R_p{}^3 = (R_p{}^3 - R_{core}{}^3)(\%V^i_{Alc} - S\Delta\%V^f_{Alc,Quasi}) + (R_{core}{}^3\%\ V^i_{EtOH}) \quad (14)$$

Using this equation, it is possible to calculate R_{core} and also R_{signal} as $R_{signal} = R_p - R_{core}$. The minimum and maximum values of R_{signal} which correspond to signal volumes for the smallest and largest droplet radius, 23 and 57 μm, are calculated to be 0.7 ± 0.2 and 1.7 ± 0.6 μm, respectively. This can be compared to $R_p - (R_p/m)$, the maximum distance into the droplet from the interface that the WGM can penetrate, which is calculated to be $\sim$6 and $\sim$14 μm for droplets of radius 23 and 57 μm, respectively. From these numbers the CERS signal is calculated to originate from the outer $\sim$3% of the droplet radius, compared to the expected region which is the outer $\sim$25% of the droplet radius. This suggests that the CERS signal may come from a region of the droplet which is much narrower than the expected $R_p - (R_p/m)$ region, illustrating that the CERS technique is more sensitive to the interfacial region than initially anticipated.

4. Concluding Remarks

Mass and heat transfer occurring during the evaporation of methanol/water, ethanol/water, and 1-propanol/water droplets has been investigated. For the former two systems, quantitative agreement between the experimental measurements and predictions from quasi-steady state theory is observed for the evolving composition of the evaporating droplets, once a scaling factor has been introduced to account for the near-surface volume probed by the spectroscopic technique. This level of consistency supports our assessment of the validity of making the quasi-steady approximation described in section 3.1, based on calculations of the time scale for gas-phase diffusion to establish a steady-state concentration profile of a species around the particle.[1] No systematic deviation with droplet size is observed, and this would be expected if the treatment was not valid. The scaling factor is required to account for the compositional gradients that occur within the evaporating droplet.

Consistent trends are also observed between the predicted change in surface temperature and the measured volume-averaged temperature, again, despite the presence of temperature gradients within the evaporating droplet that are not accounted for in the model. This suggests that this level of theory is appropriate for modeling evaporation which proceeds in a nonisothermal manner. The existence of temperature gradients is apparent in the different correlations observed between the quasi-steady surface temperature and the volume averaged measured temperature for each of the alcohol systems and for different droplet sizes, Figures 9 and 7, respectively. If the temperature profiles were the same for all systems, the correlations should be identical. That the correlations are different reflects that different systems exhibit different rates of internal energy transfer within the droplet. From an examination of the shape of the OH stretching Raman band it is possible to assess the near surface temperature and to quantify the temperature gradient within the droplet. This will provide another technique that will enable us to explore temperature profiles in more detail, and this will be discussed in detail in a subsequent publication. That both the measured and predicted compositions and temperatures are correlated suggests that the mass and heat transfer fluxes across the interface are well described by the model at early time, even if the spatial imhomogeneities in temperature and composition within the droplet are not. Consistency at longer times is yet to be tested.

The measurements of evolving temperature and composition for evaporating 1-propanol/water droplets show trends, which although self-consistent, are not correlated to the same extent with the calculated trends from quasi-steady state theory, unlike the ethanol and methanol systems. We have considered a number of possible reasons for this deviation. We have estimated that an activity coefficient for 1-propanol of $\gamma_{PrOH} = 3.3 \pm 1$ would be required to give trends consistent with the variations in composition with pressure and droplet size that are measured, a factor of 2.4 lower than the value of 7.9 measured by Butler et al.[59] It should, however, be remembered that such an activity coefficient does not resolve the apparent discrepancy between the predicted surface temperature and that measured by LIF.

We have found that within the accuracy of our experimental measurements, the scaling factor for allowing comparison of the quasi-steady predictions with experiment shows no systematic variation with droplet size. Although the quasi-steady model assumes that the concentration of the volatile components remains uniform throughout the droplets,[31] the composition of the droplets will be inhomogeneous on the time scale of our measurements as liquid phase diffusion is slow. The scaling factor allows for the fact that only a fraction of the entire droplet volume ($\sim$0.59) is probed by the CERS measurements. The scaling factor is larger than would be predicted suggesting that the CERS technique is sensitive to a narrower region nearer the droplet surface that is expected. However, this should be interpreted with caution as a number of further correction factors have not been considered in this study. These include the interaction parameter, which empirically accounts for any interaction that may occur between droplets in the droplet train as a droplet falls through the vapor field remaining from the preceding droplet.[7] In addition, although the quasi-steady model accounts for Stefan flow (radial convection), no corrections are made to the Sherwood number to account for the enhanced convective transport that can result from the relative motion of the droplet and surrounding gas phase as the droplet falls; forced

convection.[55] The former correction factor is expected to reduce the evaporation rate while the latter correction factor is expected to enhance the diffusion rate. A more extensive investigation of these correction factors will be reported in a future publication.

Acknowledgment. The authors gratefully acknowledge the financial support provided by NERC under the Core Measurements for Atmospheric Science Program. Additionally, Dr. Robert Sayer is acknowledged for assisting with preliminary measurements, Dr. Chris Howle for his input into the heat transfer measurements, and Mr. Tony Rothin for design and fabrication of the aerosol chamber.

References and Notes

(1) Seinfeld, J. H.; Pandis, S. N. *Atmospheric Chemistry and Physics: From Air Pollution to Climate* Change; John Wiley & Sons: New York City, 1998.
(2) Peter, T. *Annu. Rev. Phys. Chem.* **1997**, *48*, 785.
(3) Gogos, G.; Soh, S.; Pope, D. N. *Int. J. Heat Mass Transfer* **2003**, *46*, 283.
(4) Kunzli, N.; Kaiser, R.; Medina, S. *Lancet* **2000**, *356*, 795.
(5) Taflin, D. C.; Zhang, S. H.; Allen, T.; Davis, E. J. *AIChE J.* **1988**, *34*, 1310.
(6) Ravindran, P.; Davis, E. J. *J. Colloid Interface Sci.* **1982**, *85*, 278.
(7) Devarakonda, V.; Ray, A. K. *J. Aerosol. Sci.* **2003**, *34*, 837.
(8) Widmann, J. F.; Davis, E. J. *Aerosol Sci. Technol.* **1997**, *27*, 243.
(9) Widmann, J. F.; Heusmann, C. M.; Davis, E. J. *Colloid Polym. Sci.* **1998**, *276*, 197.
(10) Ray, A. K.; Devakottai, B.; Huckaby, J. L. *Langmuir* **1991**, *7*, 525.
(11) Kaiser, T.; Roll, G.; Schweiger, G. *Appl. Opt.* **1996**, *36*, 5918.
(12) Zhang, Y. H.; Chan, C. K. *J. Phys. Chem. A* **2002**, *106*, 285.
(13) Vehring, R.; Moritz, H.; Niekamp, D.; Schweiger, G.; Heinrich, P. *Appl. Spectrosc.* **1995**, *49*, 1215.
(14) Buehler, M. F.; Allen, T. M.; Davis, E. J. *J. Colloid Interface Sci.* **1991**, *146*, 79.
(15) Schweiger, G. *J. Aerosol Sci.* **1990**, *21*, 483.
(16) Hopkins, R. J.; Reid, J. P. *J. Phys. Chem. A* **2005**, *109*, 7923.
(17) Davis, E. J. *Aerosol Sci. Technol.* **1997**, *26*, 212.
(18) Davis, E. J.; Ray, A. K. *J. Chem. Phys.* **1977**, *67*, 414.
(19) Ray, A. K.; Davis, E. J.; Ravindran, P. *J. Chem. Phys.* **1979**, *71*, 582.
(20) Peng, C.; Chan, M. N.; Chan, C. K. *Environ. Sci. Technol.* **2001**, *35*, 4495.
(21) Choi, M. Y.; Chan, C. K. *Environ. Sci. Technol.* **2002**, *36*, 2422.
(22) Richardson, C. B.; Kurtz, C. A. *J. Am. Chem. Soc.* **1984**, *106*, 6615.
(23) Tang, I. N.; Munkelwitz, H. R.; Wang, N. *J. Colloid Interface Sci.* **1986**, *114*, 409.
(24) Choi, M. Y.; Chan, C. K. *J. Phys. Chem. A* **2002**, *106*, 4566.
(25) Ray, A. K.; Venkatraman, S. *AIChE J.* **1995**, *41*, 938.
(26) Devarakonda, V.; Ray, A. K. *J. Colloid Interface Sci.* **2000**, *221*, 104.
(27) Castanet, G.; Lebouche, M.; Lemoine, F. *Int. J. Heat Mass Transfer* **2005**, *48*, 3261.
(28) Castanet, G.; Delconte, A.; Lemoine, F.; Mees, L.; Grehan, G. *Exp. Fluids* **2005**, *39*, 431.
(29) Smolik, J.; Vitovec, J. *J. Aerosol Sci.* **1984**, *15*, 545.
(30) Chang, R.; Davis, E. J. *J. Colloid Interface Sci.* **1974**, *47*, 65.
(31) Newbold, F. R.; Amundson, N. R. *AIChE J.* **1973**, *19*, 22.
(32) Hill, S. C.; Benner, R. E. Morphology-Dependent Resonances. In *Optical Effects Associated with Small Particles*; Barber, P. W., Chang, R. K., Eds.; World Scientific: 1988; Vol. 1.
(33) Eversole, J. D.; Lin, H. B.; Huston, A. L.; Campillo, A. J.; Leung, P. T.; Liu, S. Y.; Young, K. *J. Opt. Soc. Am. B* **1993**, *10*, 1955.
(34) Sayer, R. M.; Gatherer, R. D. B.; Gilham, R.; Reid, J. P. *Phys. Chem. Chem. Phys.* **2003**, *5*, 3732.
(35) Thurn, R.; Kiefer, W. *Appl. Optics* **1985**, *24*, 1515.
(36) Thurn, R.; Kiefer, W. *Appl. Spectrosc.* **1984**, *38*, 78.
(37) Biswas, A.; Latifi, H.; Armstrong, R. L.; Pinnick, R. G. *Phys. Rev. A* **1989**, *40*, 7413.
(38) Hopkins, R. J.; Symes, R.; Sayer, R. M.; Reid, J. P. *Chem. Phys. Lett.* **2003**, *380*, 665.
(39) Symes, R.; Sayer, R. M.; Reid, J. P. *Phys. Chem. Chem. Phys.* **2004**, *6*, 474.
(40) Symes, R.; Gilham, R. J.; Sayer, R. M.; Reid, J. P. *Phys. Chem. Chem. Phys.* **2005**, *7*, 1414.
(41) Lin, H. B.; Campillo, A. J. *Opt. Lett.* **1995**, *20*, 1589.
(42) Lavieille, P.; Lemoine, F.; Lebouche, M. *Comb. Sci. Technol.* **2002**, *174*, 117.
(43) Sayer, R. M.; Gatherer, R. D. B.; Reid, J. P. *Phys. Chem. Chem. Phys.* **2003**, *5*, 3740
(44) Choi, M. Y.; Chan, C. K.; Zhang, Y. H. *J. Phys. Chem. A* **2004**, *108*, 1133.
(45) Choi, M. Y.; Chan, C. K. *J. Phys. Chem. A* **2005**, *109*, 1042.
(46) Qu, X.; Davis, E. J. *J. Aerosol. Sci.* **2001**, *32*, 861.
(47) Berglund, R. N.; Liu, B. Y. H. *Environ. Sci. Technol.* **1973**, *7*, 147.
(48) Symes, R.; Reid, J. P. *Phys. Chem. Chem. Phys.* **2005**, *in press*.
(49) Sobocinski, R. L.; Pemberton, J. E. *Langmuir* **1992**, *8*, 2049.
(50) Lemos, V.; Camargo, F. *J. Raman Spec.* **1990**, *21*, 123.
(51) Zerda, T. W.; Bradley, M.; Jonas, J. *Chem. Phys. Lett.* **1985**, *117*, 566.
(52) Mikawa, Y.; Brasch, J. W.; Jakobsen, R. J. *Spectrochimica Acta A* **1971**, *A 27*, 529.
(53) Davis, E. J.; Schweiger, G. *The Airborne Microparticle*; Springer: New York, 2002.
(54) Qu, X.; Davis, E. J.; Swanson, B. D. *J. Aerosol. Sci.* **2001**, *32*, 1315.
(55) Vesala, T.; Kulmala, M.; Rudolf, R.; Vrtala, A.; Wagner, P. E. *J. Aerosol Sci.* **1997**, *28*, 565.
(56) Chang, R.; Davis, E. J. *J. Colloid Interface Sci.* **1976**, *54*, 352.
(57) Castanet, G.; Lavieille, P.; Lebouche, M.; Lemoine, F. *Exp. Fluids* **2003**, *35*, 563.
(58) Dobson, H. J. E. *J. Chem. Soc. Trans.* **1925**, *127*, 2866.
(59) Butler, J. A. V.; Thomson, D. W.; Maclennan, W. H. *J. Chem. Soc.* **1933**, 674.
(60) *Handbook of Chemistry and Physics*; CRC Press LLC, 2003−2004; Vol. 84th Edition.
(61) Lawrence, J. R.; Glass, S. V.; Nathanson, G. M. *J. Phys. Chem. A* **2005**, *109*, 7449.
(62) Lawrence, J. R.; Glass, S. V.; Park, S. C.; Nathanson, G. M. *J. Phys. Chem. A* **2005**, *109*, 7458.
(63) Poling, B. E.; Prausnitz, J. M.; O'Connell, J. P. *The Properties of Gases and Liquids*; McGraw-Hill Book Co.: Singapore, 2001.